Reflection in a Level Set Framework for Geometric Optics *

Li-Tien Cheng †‡
Myungjoo Kang §
Stanley Osher §
Hyeseon Shim §
Yen-Hsi Tsai ¶

July 31, 2002

Abstract

Geometric optics makes its impact both in mathematics and real world applications related to ray tracing, migration, and tomography. Of special importance in these problems are the wavefronts, or points of constant traveltime away from sources, in the medium. Previously in [25], we initiated a level set approach for the construction of wavefronts in isotropic media that handled the two major algorithmic issues of resolution and multivalued solutions. This approach was quite general and we were able to construct wavefronts in the presence of refraction, reflection, higher dimensions, and, in [28], anisotropy as well. However, the technique proposed for handling reflections of waves off objects, an important phenomenon involved in all applications of geometric optics, was inefficient and unwieldy to the point of being unusable, especially in the presence of multiple reflections. We introduce here an approach based on the foundation presented in [25] that fixes this issue. This reworking fully allows the level set method to be considered for realistic applications involving geometric optics.

*Research supported by AFOSR Grant #F49620-01-1-0189

†Department of Mathematics, University of California San Diego, La Jolla, California 92093

‡Research supported by NSF Grant #0112413 and NSF Grant #0208449

§Level Set Systems Inc., 1058 Embury St., Pacific Palisades, CA 90272

¶Department of Mathematics, Princeton University, Princeton, New Jersey 08544

1 Introduction

Geometric optics consists of an approximation to high frequency wave propagation that reduces the wave equation to a static Hamilton-Jacobi equation, the eikonal equation, for the phase, or traveltime, and transport equations for the amplitude. These two quantities, phase and amplitude, compose the singular parts of the wave field and the geometric optics setting provides a simplified framework for characterizing them. Thus this approximation is fundamentally applied to numerous applications such as modern seismic data processing (see, e.g., [8, 9, 13, 14, 33]). The alternative and equivalent description of ray tracing is also widely seen and used (see, e.g., [23]).

One quantity of interest with respect to the traveltime is the wavefront. These are simply points of constant traveltime away from the sources of the waves. Thus many numerical approaches seek to construct wavefronts and hence can piece together the traveltime if so desired. These approaches will often use instead a time dependent eikonal equation whose solution at time t contains the wavefront of traveltime t away from the sources. Our interest and emphasis will mainly be on the construction of wavefronts in a time dependent setting for isotropic wave propagations. Note in isotropic media, the ray directions considered in ray tracing are equal to the local phase directions and are orthogonal to the wavefronts.

The main difficulty encountered by all numerical approaches in the construction of wavefronts in the geometric optics or ray tracing setting lies in a choice of either resolution or generation of multivalued solutions. Multivaluedness in wavefronts occur when wavefronts cross and more than one ray occupies a point in space. The formation of the well known phenomenon of caustics originates from this. Solutions obtained following the Lagrangian representation of ray tracing, which involves using the method of characteristics to track the position and ray direction of points on the wavefronts, can automatically produce multivalued wavefronts but have difficulties in resolving wavefronts in general, especially when they are diverging. On the other hand, Eulerian approaches applied to the eikonal equation automatically resolve all wavefronts over an underlying uniform grid in space but encounter difficulties in generating multivalued wavefronts. Much work has been devoted to bypassing these difficulties and the work of [34, 35, 36], for Lagrangian approaches, and [1, 5, 6, 7, 10, 16, 17, 18, 19, 20, 25, 29, 32] for Eulerian approaches, can be consulted with respect to this.

However, it was pointed out in [18] that by viewing wavefronts in phase space instead of spatial space, both difficulties could be avoided at the cost of operating on higher codimensional obejcts in a higher dimensional space.

Phase space consists of the set of (x, p), where $x \in \mathbf{R}^n$, $p \in \mathbf{R}^n$. Here, x represents the point in space and p the local phase direction. A traveltime t wavefront can be represented in this space as the set of bicharacteristic strips, which form a Lagrangian submanifold of codimension n and hence are smooth (see, e.g., [3, 4, 15, 21]). Thus operating on bicharacteristic strips has the advantage of operating with a smooth manifold, regardless of whether the projection to spatial space, which gives back the wavefronts, is multivalued or not. Furthermore, an Eulerian approach to the construction of these bicharacteristic strips set in phase space would nicely resolve them and hence the wavefronts down in spatial space. In more detail, the time dependent eikonal equation is replaced by the Liouville equation for this construction. In addition, for two dimensional geometric optics, phase space can be reduced to involve just the phase angle rather than the local phase direction. In [18], the Eulerian approach that was used involved representing bicharacteristic strips with the segment projection method, leading to a fast and efficient algorithm for the construction of wavefronts.

2 Level Set Formulation

In [25], we followed the lead of [18], operating on bicharacteristic strips, but used instead the level set method [26] for the Eulerian framework in phase space. The advantage in this was especially in simplicity. This allowed the algorithm to handle complicated wavefront evolutions without additional effort and furthermore nicely generalized to higher dimensions. The level set approach involves representing the higher codimensional bicharacteristic strips at time t by the zero level set at that time of a vector valued time dependent level set function existing in phase space. The Liouville equation on each component, written as

$$u_t + v \cdot \nabla_{x,p} u = 0,$$

where u is such a component and v comes from the ray tracing directions or, equivalently, the characteristics of the eikonal equation, can then be used to generate the bicharacteristic strips and, ultimately, the wavefronts of interest. It will be useful to note that for two dimensional geometric optics, where we can operate in reduced phase space, the two components, ϕ and ψ, of the vector valued level set function satisfy the system

$$\begin{aligned} \phi_t + v \cdot \nabla_{x,\theta} \phi &= 0, \\ \psi_t + v \cdot \nabla_{x,\theta} \psi &= 0, \end{aligned}$$

where θ denotes the phase angle, v is given by

$$v(x,\theta) = \begin{pmatrix} c(x)\cos\theta \\ c(x)\sin\theta \\ c_{x_1}(x)\sin\theta - c_{x_2}(x)\cos\theta \end{pmatrix},$$

and $c > 0$ is the given local wave velocity permitted in the medium. Also note these two transport equations in ϕ and ψ can be solved separately. As the quantites of interest are now redefined into phase space, or the reduced version, a fixed, uniform grid can be placed there over which we can obtain numerical solutions. This grid provides the automatic resolution desired.

Thus the steps of the algorithm for constructing the traveltime t wavefront involve producing the vector valued level set function that corresponds to the given initial wavefront, solving the Liouville partial differential equations (PDE's) up to time t, and outputting the projection of the zero level set to spatial space. Herein lies the simplicity of the approach. We note that additional steps are usually taken during the solving step of the PDE's in a process called reinitialization to enforce a stable form for the vector valued level set function. This, though, is not needed for a medium of constant index of refraction, i.e., when c is constant. We refer to [25] for details of this and the algorithm in general as we are concerned here with other aspects.

3 Reflections

In fact, our interest lies in the case where there are objects in the medium that can reflect wavefronts. Reflection was considered in [25] as well but the approach introduced there could become unreasonably inefficient when multiple reflections occur. This is because the approach consists of creating more vector valued level set functions to represent wavefronts each time they are reflected. Further details include interface boundary conditions on the object surface to enforce Newton's law of reflection. Nevertheless, dealing with all these level set functions, which can add up without bound, can be unwieldy. This is a major drawback as reflections of waves occur all the time in the real world and serve an important purpose in numerous applications such as ray tracing and scattering (see, e.g., [11]). Thus, our goal here is, building upon the established level set framework for geometric optics, to introduce and implement a technique that handles reflections in a more realistic and efficient way.

We consider the model problem where the objects are given and no waves can exist in their interiors. This time, our approach is to use one

vector valued level set function to represent all wavefronts, reflected or not. The reflecting objects, which can be given in spatial space through a level set function $\tilde{\rho}(x)$ as $\{\tilde{\rho} \leq 0\}$, are extended to phase space and represented by $\{\rho \leq 0\}$, where $\rho(x,p) = \tilde{\rho}(x)$. We can in fact require that $\tilde{\rho}$ and ρ are distance functions with respect to their zero level sets in their respective spaces. Furthermore, we will frequently refer to both $\{\tilde{\rho} = 0\}$ in spatial space and $\{\rho = 0\}$ in phase space, or reduced phase space, as object boundaries. Away from the objects, wavefront evolution is as before, satisfying the relevant Liouville equations. The interesting behavior happens, of course, near the objects. At the boundary, we wish to pose boundary conditions that will enforce reflection.

For simplicity, we first consider the case of geometric optics in two dimensions in a medium of constant index of refraction and discuss generalizations later. This means the Liouville PDE's take the abbreviated form

$$\begin{aligned} \phi_t + (c\cos\theta)\phi_{x_1} + (c\sin\theta)\phi_{x_2} &= 0, \\ \psi_t + (c\cos\theta)\psi_{x_1} + (c\sin\theta)\psi_{x_2} &= 0, \end{aligned}$$

and derivatives in the θ-direction are absent. We will use a formula that relates an incoming ray that strikes the object to the subsequent reflected ray. Let θ_I be the angle of the ray that strikes the object. Also let θ_B denote the outward normal of the object boundaries, which are curves, at the point of striking. Then the angle, going counterclockwise, from the incoming ray to the normal at the interface, denoted by β_I, is equal to $\theta_B - \theta$. Newton's law for reflection says that if β_R furthermore denotes the angle from the reflected ray to the normal at the interface, then $\beta_I = \pi - \beta_R$. Thus we get that β_R should equal to $\pi - (\theta_B - \theta_I)$. In terms of the angle θ_R of the reflected ray, we have $\beta_R = \theta_B - \theta_R$ and so $\theta_R = 2\theta_B - \theta_I - \pi$. Note this condition was also used in [25] to link together the different vector valued level set functions.

To use this in our level set framework, we notice that since we are considering isotropic media, the values of θ on bicharacteristic strips give the angles of the normals to the corresponding wavefronts, which are exactly the angles of the ray directions. According to our analysis, given x in spatial space lying on the object boundaries and any θ, the value of our vector valued level set function at (x,θ) for any time t should equal to the value at $(x, 2\theta_B - \theta - \pi)$, where θ_B is the angle of the normal of the object boundaries at x. Note that one of these points has an incoming ray, in terms of the characteristics of the Liouville PDE's, and the other has a reflected ray. The one with the incoming ray will get its value from the Liouville

PDE, which should then be copied to the other point to enforce reflection. Thus especially, if the bicharacteristic strips of interest, which are a part of the vector valued level set function, hit the object boundaries, reflected bicharacteristic strips will be created in the function moving in the correct direction and manner. We will later write down a criterion for determining which points get their information from incoming rays, i.e., from the Liouville PDE, and which from reflected rays, i.e., from reflection boundary conditions. So the evolution step of the algorithm consists of solving the Liouville PDE's in the region in reduced phase space exterior to the objects, i.e., $\{\rho > 0\}$, which we term the computational region, with the above serving as boundary conditions on the object boundaries, i.e., $\{\rho = 0\}$.

4 Numerical Discretization

In the implementation of this approach, since we are building upon the framework of [25], we employ the same numerical setting. Thus, we operate on a uniform grid in three dimensional reduced phase space. As mentioned before, this grid, along with the properties of self interpolation afforded by a PDE approach, allows for automatic resolution of wavefronts.

Before we consider the technique for numerically solving the relevant Liouville PDE's, we first clarify some points and present the discretization of certain basic quantities that will be used later. First, an initial vector valued level set function is chosen that not only represents the initial given wavefronts but also satisfies the boundary conditions on the object boundaries. These boundary conditions will be preserved under the evolution of the level set function. For the second point, we note that the computation of the quantity θ_B can be determined from the well known formula for normals in a level set framework, $\frac{\nabla\tilde{\rho}}{|\nabla\tilde{\rho}|}$, giving

$$\theta_B = \arctan \frac{\tilde{\rho}_{x_2}}{\tilde{\rho}_{x_1}}.$$

The actual value for this expression can be computed through finite differencing for the derivatives and interpolation over the grid. Note also that the formula for normals, and thus also θ_B, exists at all points x in space. In fact, this expression produces the normal of the particular level set surface passing through the point x. Finally, the location of the object boundaries can be accurately computed through interpolation to find the zeros of ρ and the interior and exterior of the objects are determined by the sign of ρ.

This leads us to the discretization of the Liouville PDE's to arrive at the vector valued level set function at a desired time. The spatial discretization involved needs to adapt the correct boundary conditions at the object boundaries. The time discretization, however, may be the same everywhere and Total Variation Diminishing Runge-Kutta methods [30] (TVD-RK), or even Strong Stability Preserving Runge-Kutta methods [31] (SSP-RK), of high order can be used. In our simulations, we simply employ Forward Euler since our current spatial discretization, which is discussed below, is first order accurate anyway. For the spatial discretization in reduced phase space, away from object boundaries, we may use high order upwind methods such as Essentially Non Oscillatory [30] (ENO) and Weighted Essentially Non Oscillatory [22] (WENO) schemes, as in [25]. However, since we will, for simplicity, be modifying first order upwinding near the object boundaries, we use first order upwinding away from object boundaries as well. Though this only allows first order accuracy, the advantage is in simplicity and fast computations. We do note that we are currently working on achieving higher order accuracy.

For grid points next to object boundaries, first order upwinding is attempted but needs to be modified according to the availability of information. We illustrate the discretization in an example with a one dimensional spatial space $[0, \infty)$ with a reflecting wall occupying $[0, a]$, for some $a > 0$. Notice there can only be two phase angles, $\theta = 0, \pi$. Given a uniform grid over spatial space denoted by the collection of $0 = x_0 < x_1 < x_2 < \dots$ with stepsize Δx, the grid over reduced phase space consists of (x_i, θ_j), $i = 0, 1, 2, \dots$ and $j = 0, 1$, where $\theta_1 = 0$ and $\theta_2 = \pi$. This is a slight abuse of notation as x_i was previously used to denote coordinates of a spatial point x, however, there is no confusion for this example. Let x_k denote the grid point in spatial space closest to but greater than a and suppose $x_k \neq a$. Thus there exists $0 < \mu < 1$ such that $x_k - a = \mu \Delta x$. See Figures 1 and 2 for clarification. We start with a function u_0 defined in reduced phase space in the computational region, $x \in (a, \infty)$, and consider the model equation

$$u_t + (c \cos\theta) u_x = 0,$$

with $u = u_0$ at $t = 0$. Thus the function will travel to the left for $\theta = \pi$ and when it hits the wall, it will reflect, reappearing at $\theta = 0$ and moving to the right. Note u and the model equation take the place of ϕ or ψ and its corresponding Liouville equation.

As we mentioned before, at grid points away from a, first order upwinding can be applied without problems to the discretization of u_x. However,

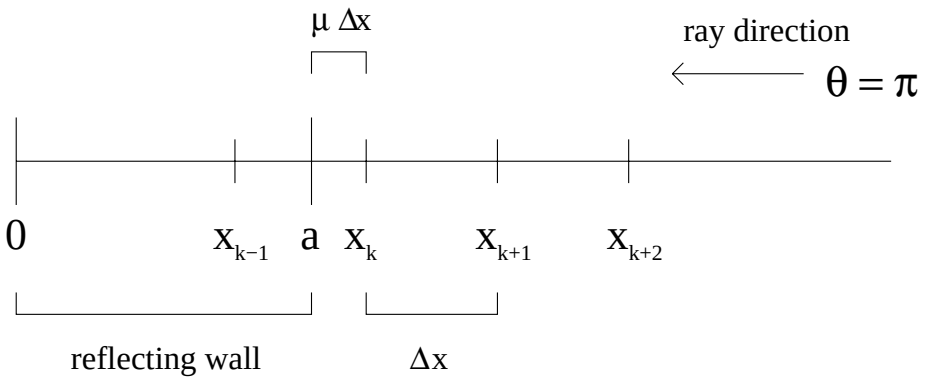

Figure 1: This diagram shows the $\theta = \pi$ slice and labels the reflecting wall, ray direction, and grid points near the wall.

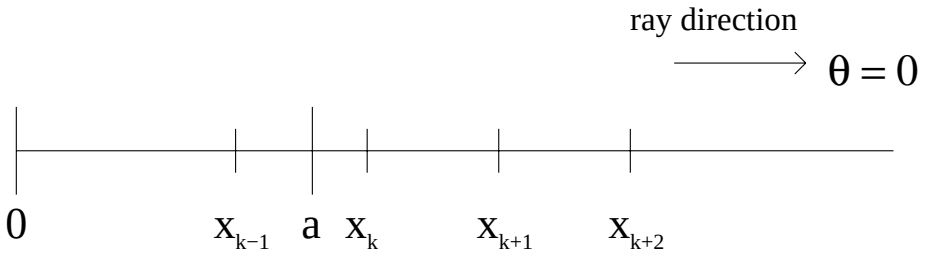

Figure 2: This diagram shows the $\theta = 0$ slice with grid points and ray direction.

at x_k, care must be taken since x_{k-1} is in the interior of the reflecting wall and thus u has no real value there. The value at x_{k-1}, though, is possibly not used depending on the what the correct upwinding direction is. Note, at $\theta = \pi$, first order upwinding uses $u(x_k, \pi, t)$ and $u(x_{k+1}, \pi, t)$, which are defined. However, at $\theta = 0$, first order upwinding over the grid attempts to use $u(x_k, 0, t)$ and, unfortunately, $u(x_{k-1}, 0, t)$. In this case, instead of $u(x_{k-1}, 0, t)$, we can use $u(a, 0, t)$, which should be derivable from the reflection boundary condition. In an alternate description, this is because for $\theta = \pi$, the ray at x_k, and also a, is an incoming ray and so information passed from the region should be used. But for $\theta = 0$, the rays at x_k and a come from reflected rays and so information passed from the boundary should be used. Note at a, $\theta_B = 0$ and so, as expected, an incoming ray with angle π reflects to the angle -2π, which is the same as 0. Thus $u(a, 0, t)$ can be obtained from the value of u at $x = a$ and $\theta = \pi$. This information is provided by the incoming ray from within the region. The value of u at this boundary location can be obtained from extrapolation on the values at the nearby points (x_k, π) and (x_{k+1}, π). Then u at $\theta = 0$ can use this information.

A final note in this example is in terms of efficiency. If u_x at $\theta = 0$ and $x = x_k$ is discretized using first order upwind differencing and the information at a, the resulting algorithm will be restricted by the stability condition $\Delta t < \frac{\mu \Delta x}{2}$ when using Forward Euler in time, where Δt denotes the time step. This can be unduly restrictive if μ is small. Thus we modify the approach so that when $\mu \geq \frac{1}{2}$, we keep this discretization, but when $\mu < \frac{1}{2}$, we skip x_k and compute u at x_{k+1} with a first order upwind method using x_{k+1} and the point on the wall, a, which are separated by more than Δx. Then if a value for u is actually wanted at x_k, it can be computed from interpolation or extrapolation once the value of u has been determined elsewhere, for example, from the values at x_{k+1} and a. The CFL condition is thus $\Delta t < \frac{\Delta x}{4}$, which does not depend on μ and is not overly stringent.

For two dimensional spatial space, we follow the same philosophy. For grid points next to the object boundaries, if first order upwind differencing does not involve differencing across the object boundaries, then this approximation is used since the information at that point comes from an incoming ray. On the other hand, at grid points where differencing is attempted across the object boundaries, boundary points are used instead in the approximation, as in the one dimensional case. However, in this case, the boundary points involved may get their values from incoming rays rather than only from the reflection boundary condition (see Figure 3). We may use the di-

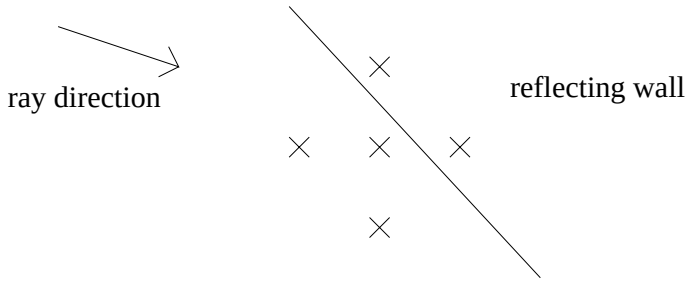

Figure 3: This diagram shows a slice in reduced phase space of a grid point of interest surrounded by its spatial neighbors. The phase angle of the slice is shown as a ray direction. First order upwinding at this point will attempt to use values at the neighboring points to the left and above it, even though the ray here is an incoming ray and the point above the point of interest is within the reflecting wall to the right.

rection of the outward normal vector, $\nabla\tilde{\rho}$, and the ray direction considered, which has angle θ, at the point to determine where it gets its value. The condition to check is whether at the point,

$$\tilde{\rho}_{x_1}\cos\theta + \tilde{\rho}_{x_2}\sin\theta,$$

the dot product between the ray and normal directions, is greater than or less than zero. If it is less than zero, then the ray there is an incoming ray. Thus, the value can be gathered through extrapolation involving nearby grid points. If the above is greater than zero, however, then the value at the point should come from the reflection boundary conditions, i.e., from the value of the boundary point at the same spatial location but with phase angle $2\theta_B - \theta - \pi$ which has an incoming ray and thus a determined value. A final detail is when searching for the correct angle of the incoming ray that will prescribe the reflection boundary condition at an object boundary point, this angle may not be one of the discrete values for the phase angle taken in the grid. This means even if θ is a discrete value of the phase angle of the grid, $2\theta_B - \theta - \pi$ may not be. In this case, interpolation can be used with nearby angles available in the grid to fill in this information. This forms the discretization we use for the Liouville PDE's of our level set functions.

With this, we can solve the Liouville PDE's for ϕ and ψ up to any given time t. To obtain the traveltime t wavefront, recalling our method of representation, we may use interpolation techniques such as those related to

[24] to obtain the intersection of the zero level sets of ϕ and ψ. This gives the bicharacteristic strips which can be projected to arrive at the wavefront of interest. See [12] and [25] for more details on this.

5 Numerical Simulations

Currently, we have mainly applied our algorithm to the case of reflecting walls at the spatial boundaries. Thus if we are working in the domain $[-1,1] \times [-1,1]$ in spatial space, then the reflecting walls are located at a choice of $x_1 = \pm 1$ and $x_2 = \pm 1$. This simplifies a lot of our previous calculations. Figure 4 shows an expanding circle in a medium of index of refraction 1 in such a setting with four reflecting walls using our algorithm. As time increases, more and more reflections take place, leading to wavefronts that almost fill up spatial space. Note our approach not only handles the multiple reflections, which lead to complicated multivalued solutions, but resolves well the wavefronts which have grown tremendously in length. Figure 5 shows the continuation of the previous simulation up to even larger time. Multiple reflections, multivalued solutions, and resolution are taken care of with ease. Figures 6,7, and 8 show the bicharacteristic strips in reduced phase space computed at different times. Notably, the simple curve of Figure 6 shows the bicharacteristic strips that form the initial circle and Figures 6 and 7 show them for wavefronts that have undergone more and more reflections. Note though there are many curve segments in the pictures, they are all smooth, even when their projection contains many intersections. Also, the figures are plotted with the phase angle $[-\pi, \pi]$ mapped into $[-1, 1]$ for simplification. Finally, for illustration, we show the level set functions involved in Figures 6, 7, and 8 in Figures 9, 10, and 11, respectively.

Figure 12 shows an initially small growing ellipse in a domain with a single reflecting wall at $x_1 = 1$. The ellipse expands and reflects off the wall while passing through the boundary at $x_2 = -1$. Note a sharp reflection wavefront is generated and resolved without problems.

Finally, Figure 13 considers a single reflecting wall at the left slanting from top left to bottom right that does not align with the grid. The original wavefront, moving downwards, is the horizontal straight line at the top, linking up with the corresponding reflected line at the wall. These are drawn into the reflecting wall but those portions can be ignored in the plot. In this case, we performed a simplification as the incoming and reflected wavefronts will always be straight lines with slopes preserved throughout the evolution. Thus, we consider just two phase angles in reduced phase

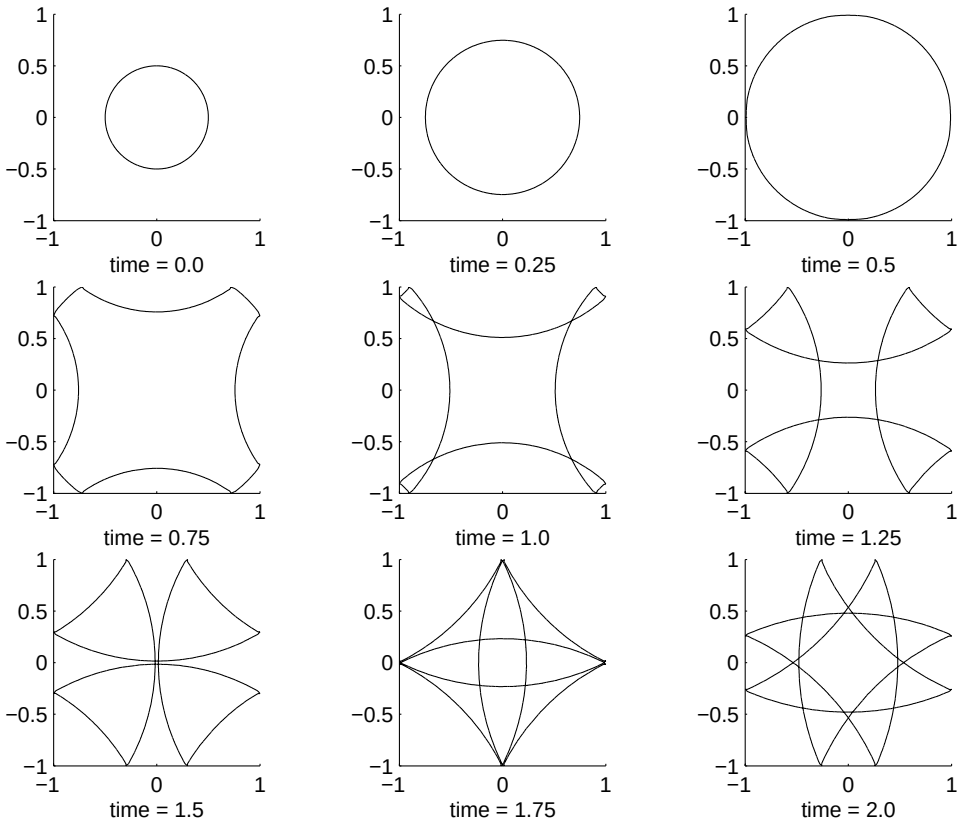

Figure 4: This figure shows an initially growing circular wavefront that subsequently reflects multiple times off four walls forming a box.

space, the ones corresponding to the incoming and reflected wavefronts. Furthermore, we just need one level set function and plot the projection into spatial space of the zero level sets at each of the two phase angles to arrive at the wavefronts of interest. As seen from the figure, our algorithm is able to capture these wavefronts as they evolve and reflect. This example still serves as a verification of our approach even though it has been simplified since many of fundamental elements, such as the discretization of the Liouville PDE, are preserved in the simplification.

We are currently working on simulations involving more complicated object boundaries in a general setting. However, the ones we have so far already show a vast improvement over the previous approach found in [25].

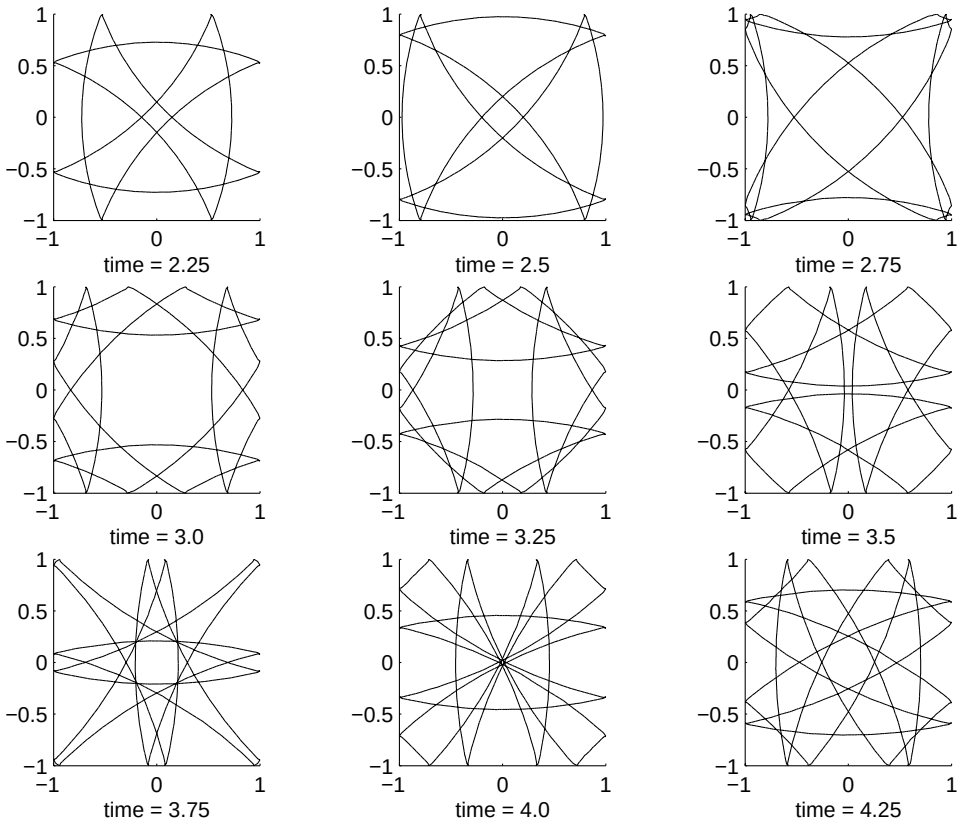

Figure 5: This figure continues that of Figure 4, showing even more reflections with a final wavefront taking up much of the computational region.

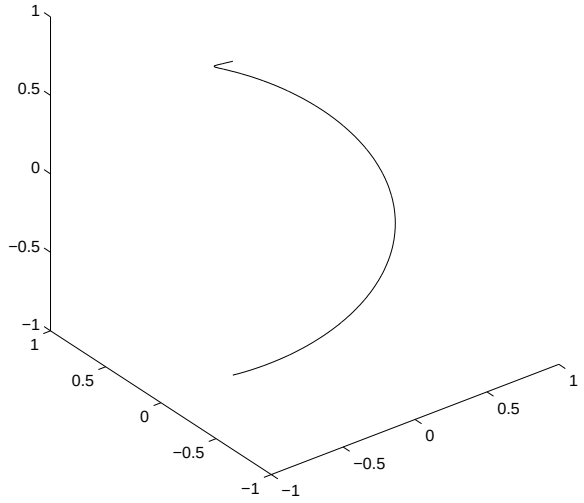

Figure 6: This figure shows the bicharacteristic strips in reduced phase space associated to the initial circular wavefront.

6 Generalizations

We would of course like to generalize our approach to anisotropic wave propagations, which was handled under a level set approach in [28], as well as variable indices of refraction, and three dimensional spatial space. Variable index of refraction would not seem to present too many problems since this would only include the term with the θ-derivative in the Liouville equations. These derivatives should not be hard to discretize since the interior and exterior of the objects are determined by the spatial location only. Some details need to be handled with respect to reinitialization though and we plan to discuss this in future work.

As for three dimensional spatial space, in [25], we wrote down a relationship between incoming rays and reflected rays, namely that

$$C = -B + 2\frac{(B \cdot A)A}{|A|^2},$$

where A is the normal vector to the interface at the point of reflection, B is the incoming ray, and C is the reflected ray. Incorporating this would form the first steps for an algorithm for three dimensions. Care, however, would

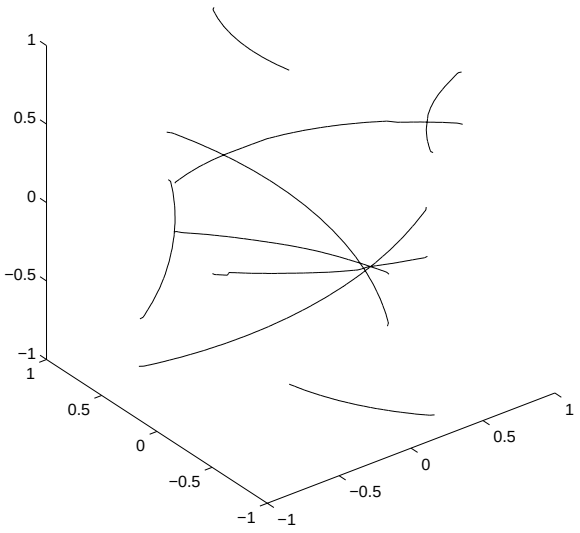

Figure 7: This figure shows the bicharacteristic strips in reduced phase space associated to the initial circular wavefront at a later time, after reflections have occurred.

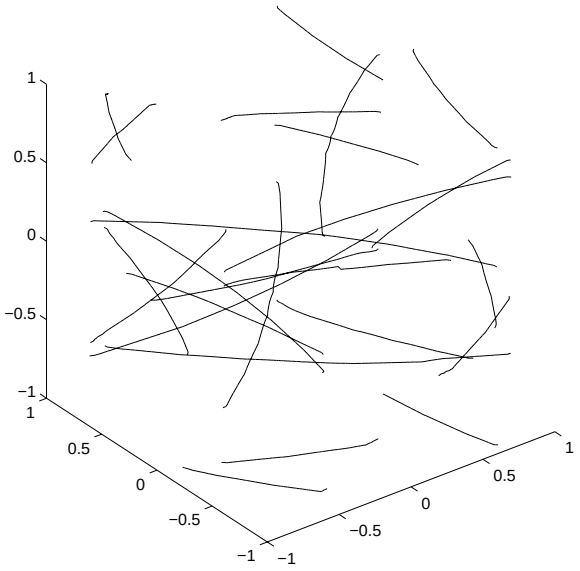

Figure 8: This figure shows the bicharacteristic strips in reduced phase space associated to the initial circular wavefront at a later time. Note the bicharacteristic strips are smooth even after the multiple reflections involved.

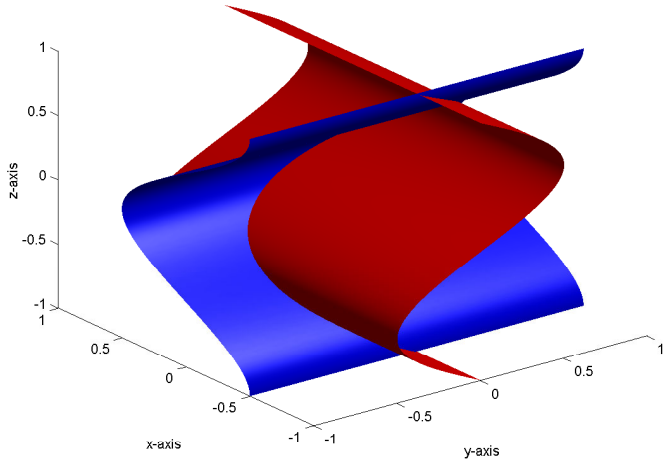

Figure 9: This figure shows the zero level sets of the two components of the vector valued level set function involved in Figure 6. The intersection of the two surfaces gives the bicharacteristic strips.

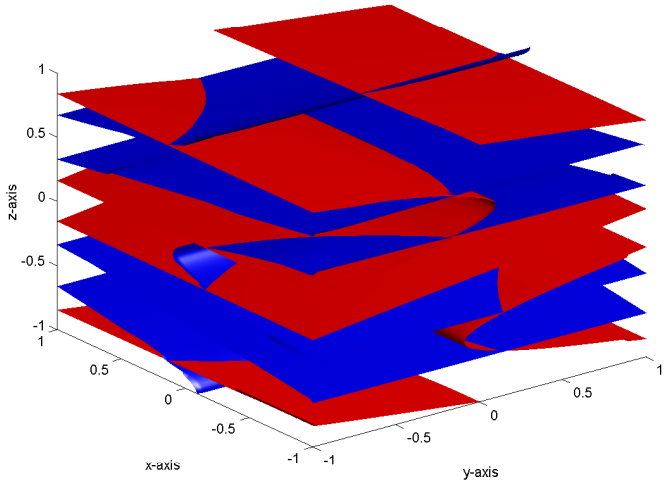

Figure 10: This figure shows the zero level sets of the two components of the vector valued level set function involved in Figure 7.

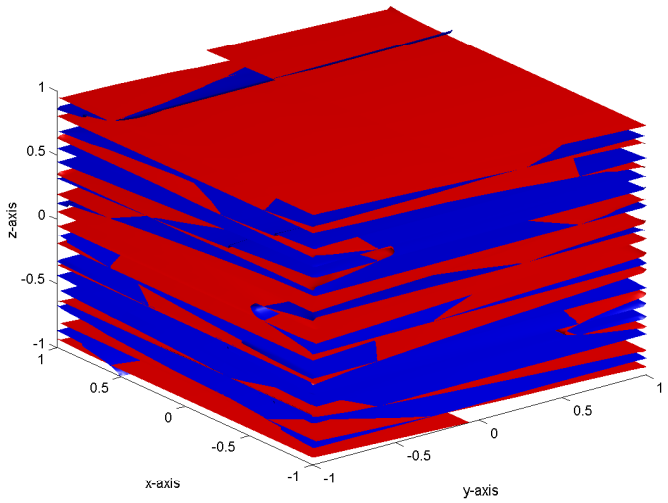

Figure 11: This figure shows the zero level sets of the two components of the vector valued level set function involved in Figure 8.

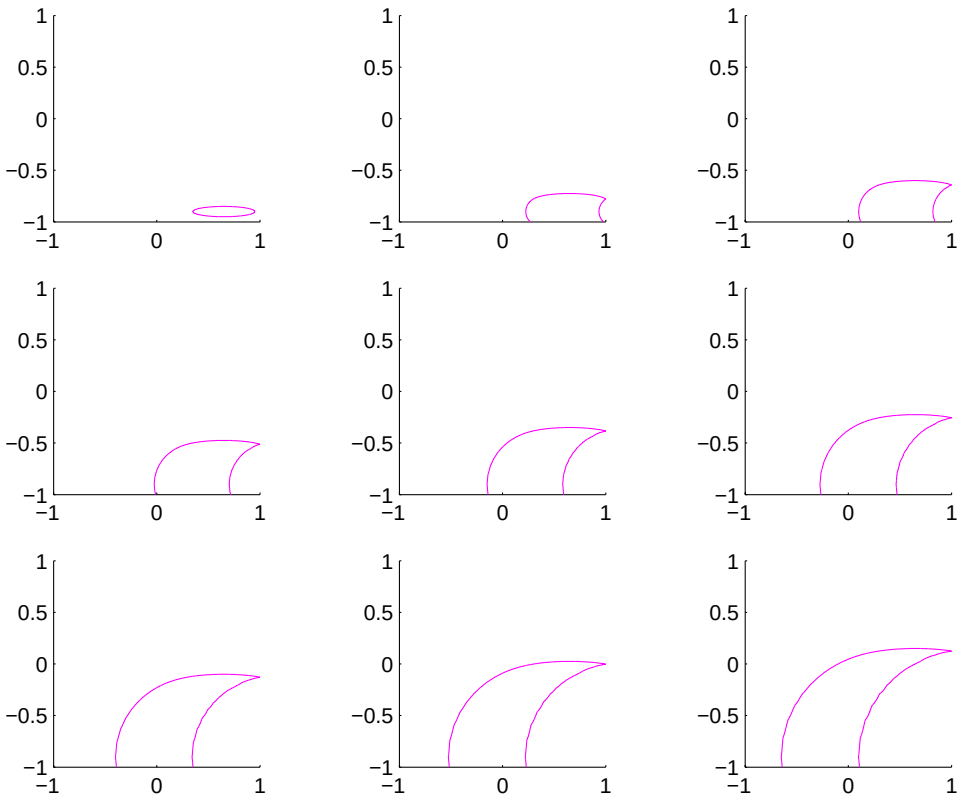

Figure 12: This figure shows an initially small growing ellipse reflecting off a wall at $x_1 = 1$.

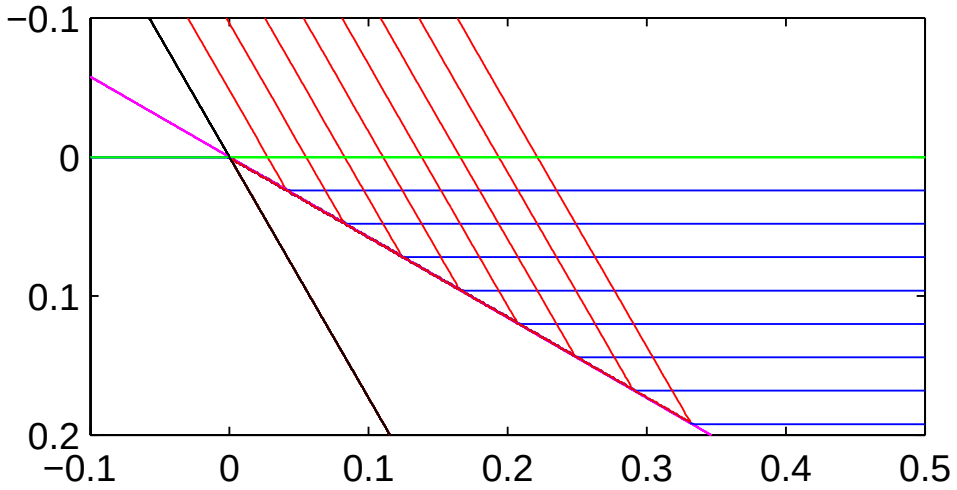

Figure 13: This figure shows an initial downward moving horizontal wavefront with the corresponding reflected portion in a medium with a slanted reflecting wall not aligned with the grid.

need to be taken in terms of efficiency, possibly with local level set methods (see, e.g., [2, 12, 25, 27]), since phase space in this case is six dimensional.

7 Conclusion

Building upon the setting of [25], we were able to introduce an approach that can handle reflections of waves in a reasonable and efficient manner while preserving the benefits afforded by the previous work, notably with respect to resolution and multivalued solutions. This is a great improvement over the previous attempt found in [25] and is needed if realistic cases of wave propagation are to be considered. We are currently working on further generalizing our algorithm to handle anisotropy, variable indices of refraction, and a three dimensional spatial space.

References

[1] R. Abgrall and J.-D. Benamou. Big Ray Tracing and Eikonal Solver on Unstructured Grids: Application to the Computation of a Multivalued Travel-Time Field in the Marmousi Model. *Geophysics*, 64:230–239, 1999.

[2] D. Adalsteinsson and J.A. Sethian. A Fast Level Set Method for Propagating Interfaces. *J. Comput. Phys.*, 118:269–277, 1995.

[3] V.I. Arnol'd. *Catastrophe Theory.* Springer-Verlag, 1992.

[4] V.I. Arnol'd, S.M. Gusein-Zade, and A.N. Varchenko. *Singularities of Differential Maps.* Birkhauser, 1986.

[5] J.-B. Benamou. An Eulerian Numerical Method for Geometric Optics. To appear in COCV Proc.

[6] J.-D. Benamou. Big Ray Tracing: Multi-Valued Travel Time Field Computation Using Viscosity Solutions of the Eikonal Equation. *J. Comput. Phys.*, 128:463–474, 1996.

[7] J.-D. Benamou. Direct Solution of Multi-Valued Phase-Space Solutions for Hamilton-Jacobi Equations. *Comm. Pure Appl. Math.*, 52, 1999.

[8] G. Beylkin. Imaging of Discontinuities in the Inverse Scattering Problem by Inversion of a Causal Generalized Radon Transform. *J. Math. Phys.*, 26:99–108, 1985.

[9] G. Beylkin and R. Burridge. Linearized Inverse Scattering Problem of Acoustics and Elasticity. *Wave Motion*, 12:15–22, 1990.

[10] Y. Brenier and L. Corrias. A Kinetic Formulation for Multi-Branch Entropy Solutions of Scalar Conservation Laws. *Ann. IHP Analyse non-lineaire*, 1996.

[11] Oscar Bruno. New high-order, high-frequency integral methods in computational electromagnetism. 2002.

[12] P. Burchard, L.-T. Cheng, B. Merriman, and S. Osher. Motion of Curves in Three Spatial Dimensions Using a Level Set Approach. *J. Comput. Phys.*, 170(2):720–741, 2001.

[13] R. Burridge, M.V. de Hoop, D. Miller, and C. Spencer. Multiparameter Inversion in Anisotropic Media. *Geophys. J. Internat.*, 134:757–777, 1998.

[14] M.V. de Hoop and N. Bleistein. Generalized Radon Transform Inversions for Reflectivity in Anisotropic Elastic Media. *Inverse Problems*, 13:669–690, 1997.

[15] J.J. Duistermaat. Oscillatory Integrals, Lagrange Immersions and Unfolding of Singularities. *Comm. Pure Appl. Math.*, 27:207–281, 1974.

[16] B. Engquist, E. Fatemi, and S. Osher. Numerical Resolution of the High Frequency Asymptotic Expansion of the Scalar Wave Equation. *J. Comput. Phys.*, 120:145–155, 1995.

[17] B. Engquist and O. Runborg. Multi-Phase Computation in Geometrical Optics. Tech Report, Nada KTH, 1995.

[18] B. Engquist, O. Runborg, and A.-K. Tornberg. High Frequency Wave Propagation by the Segment Projection Method. CAM Report 01-13, UCLA, 2001.

[19] M. Fang, J. Steinhoff, and L. Wang. A New Eulerian Method for the Computation of Propagating Short Acoustic and Electromagnetic Pulses. To appear in J. Comput. Phys.

[20] S. Fomel and J.A. Sethian. Fast Phase Space Computation of Multiple Arrivals. Technical Report LBNL-48976, LBL, 2001.

[21] S. Izumiya. The Theory of Legendrian Unfoldings and First Order Differential Equations. *Proc. Royal Soc. Edinburgh*, 123A:517–532, 1993.

[22] G.S. Jiang and D. Peng. Weighted ENO Schemes for Hamilton Jacobi Equations. *SIAM J. Scient. Comput.*, 21(6):2126–2143, 2000.

[23] Peter D. Lax. Asymptotic solutions of oscillatory initial value problems. *Duke Math. J.*, 24:627–646, 1957.

[24] W.E. Lorenson and H.E. Cline. Marching cubes: A high resolution 3D surface reconstruction algorithm. *Comp. Graphics*, 21(4):163–169, 1987.

[25] S. Osher, L.-T. Cheng, M. Kang, H. Shim, and Y.-H. Tsai. Geometric Optics in a Phase Space Based Level Set and Eulerian Framework. *J. Comput. Phys.*, 179:622–648, 2002.

[26] S. Osher and J.A. Sethian. Fronts Propagating with Curvature Dependent Speed: Algorithms Based on Hamilton-Jacobi Formulations. *J. Comput. Phys.*, 169(1):12–49, 1988.

[27] D. Peng, B. Merriman, S. Osher, H. Zhao, and M. Kang. A PDE-Based Fast Local Level Set Method. *J. Comput. Phys.*, 155(2):410–438, 1999.

[28] J. Qian, L.-T. Cheng, and S. Osher. A Level Set Based Eulerian Approach for Anisotropic Wave Propagations. Submitted to Wave Motion.

[29] S.J. Ruuth, B. Merriman, and S. Osher. Fixed Grid Method for Capturing the Motion of Self-Intersecting Interfaces and Related PDEs. *J. Comput. Phys.*, 163:1–21, 2000.

[30] C.W. Shu and S. Osher. Efficient Implementation of Essentially Nonoscillatory Shock-Capturing Schemes. *J. Comput. Phys.*, 77(2):439–471, 1988.

[31] R.J. Spiteri and S.J. Ruuth. A New Class of Optimal High-Order Strong-Stability-Preserving Time Discretization Methods. To appear in SINUM.

[32] W.W. Symes. A Slowness Matching Finite Difference Method for Traveltimes Beyond Transmission Caustics. The Rice Inversion Project Annual Report, Rice University, 1996.

[33] W.W. Symes and J.J. Carazzone. Velocity Inversion by Differential Semblance Optimization. *Geophysics*, 56:654–663, 1991.

[34] V. Vinje, E. Iversen, K. Astebol, and H. Gjøystdal. Estimation of Multivalued Arrivals in 3D Models using Wavefront Construction–Part I. *Geophysical Prospecting*, 44:819–842, 1996.

[35] V. Vinje, E. Iversen, K. Astebol, and H. Gjøystdal. Part II: Tracing and Interpolation. *Geophysical Prospecting*, 44:843–858, 1996.

[36] V. Vinje, E. Iversen, and H. Gjøystdal. Traveltime and Amplitude Estimation using Wavefront Construction. *Geophysics*, 58(8):1157–1166, 1993.